Composites Part B 87 (2016) 263–273

Contents lists available at ScienceDirect

Composites Part B

journal homepage: www.elsevier.com/locate/compositesb

Probabilistic strength based matrix crack evolution in multi-directional composite laminates

N. Jagannathan [a, b], S. Gururaja [b, *], C.M. Manjunatha [a]

[a] Structural Technologies Division, CSIR-National Aerospace Laboratories, Bangalore, 560017, India
[b] Department of Aerospace Engineering, Indian Institute of Science, Bangalore, 560012, India

ARTICLE INFO

Article history:
Received 30 March 2015
Received in revised form
24 August 2015
Accepted 27 September 2015
Available online 3 November 2015

Keywords:
A. Polymer-matrix composites (PMCs)
B. Damage tolerance
C. Analytical modelling
Matrix cracking

ABSTRACT

Matrix cracking is the first and most dominant mode of damage in laminated polymer composites resulting in significant stiffness degradation. In the past, matrix cracking has been quantified using crack density evolution with loading and correlating the crack densities with stiffness degradation of the laminate. In the present study, an analytical framework for matrix crack evolution for a general Multi-Directional (MD) symmetric laminate has been proposed using oblique coordinate based shear-lag analysis coupled with a probabilistic strength approach. The statistical parameters have been estimated from a master laminate. The ply-by-ply crack density evolution has also been simulated. The crack density evolution and associated stiffness degradation predictions have been compared to existing experimental values. The stiffness degradation trends closely match with experimental data and stiffness values estimated from current approach are conservative.

1. Introduction

The use of Fiber Reinforced Polymer (FRP) composites for structural load bearing applications has increased in recent times. Approximately 50% by weight of the recent Boeing 787 airframe is made from FRPs [1]. Over the next few decades, these materials are likely to replace conventional materials due to their high specific strength, stiffness, corrosion resistance, easy formability and much greater fatigue life [2]. During service, composite structures are subjected to time varying events of loading, environment degradation, damage events such as bird impact, runway debris, hail-storm, etc., acting individually or sometimes in combination. Due to the inherent inhomogeneity and distinctly anisotropic nature, FRPs exhibit a multitude of damage mechanisms such as matrix cracking, interfacial fiber-matrix debonding, fiber breaks, delamination, fiber micro-buckling etc. under static and fatigue loading. Damage typically starts very early during loading and evolves steadily [3,4]. Matrix cracking happens to be the most dominant mode of damage to first appear in the laminate [4,5]. Typically, matrix cracks initiates in the lamina making the maximum off-axis angle with the loading direction. When the laminate is viewed in thickness direction, the matrix cracks appear transverse to the loading direction and propagate along the fiber direction of the off-axis ply (as shown in Fig. 1 (a)). As the static loading increases or as the number of cycles increase in case of fatigue, the matrix crack density (i.e., the number of matrix cracks per unit length) attains a saturation state called Characteristic Damage State (CDS) [6]. Since matrix crack evolution in composite laminates is accompanied by stiffness degradation, it becomes important to model this phenomenon.

Experimental investigation of crack initiation and evolution is mostly limited to cross-ply or Quasi-Isotropic (QI) laminates [7–11]. Notable observations from experimental studies on matrix cracking are as follows:

1. During matrix cracking, there occurs a continuous loss of stiffness, stress redistribution and reduction in stress concentration. Other damage modes such as delamination are also triggered when it attains CDS [3,4].
2. Matrix cracks form instantaneously through the laminate width along the fiber direction and are referred to as tunneling cracks. However, more complex cracking like partial cracking has been observed in plies adjacent to 90° ply [9,10].
3. The applied far field strain magnitude causing matrix crack initiation in a particular off-axis ply increases with decrease in ply thickness as well as with increase in neighboring ply

* Corresponding author.
E-mail address: suhasini@aero.iisc.ernet.in (S. Gururaja).

http://dx.doi.org/10.1016/j.compositesb.2015.09.050
1359-8368/

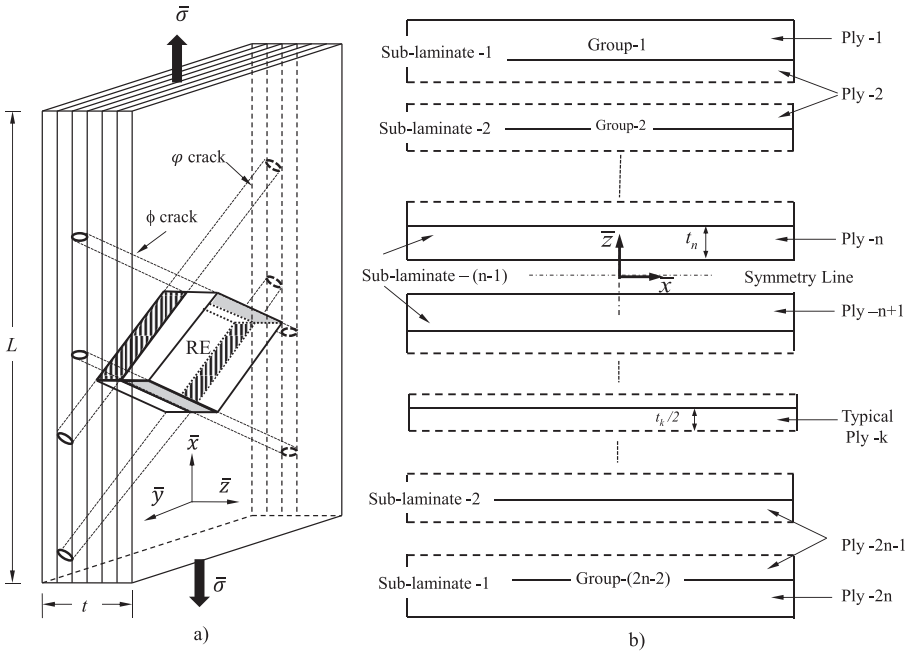

Fig. 1. Matrix cracking in MD-laminate. a) Representative element, b) Sub-laminate concept.

thickness [12–16]. In other words, the neighboring plies provide a 'constraint' effect and matrix cracking initiation becomes dependent on the location of the ply under consideration with respect to the overall stacking sequence of plies. Thus, matrix crack initiation strain for surface plies are found to be lower than for plies located in between other plies.

4. Saturation matrix crack density at CDS decreases with increase in the ply thickness or with increase in constraint ply thickness [11].
5. The matrix crack initiation strain is higher for plies with off-axis angle less than 90° and curved crack paths are also observed [17,18].
6. For MD-laminate containing plies with off-axis angle less than 45°, the laminate fails before any matrix cracks form in that ply and offers limited contribution to overall stiffness reduction of the laminate [8,19].

Over the last three decades, numerous matrix crack initiation and evolution models have been developed to predict matrix crack density evolution under a given loading scenario. Starting with basic 1-D shear lag analysis extended for crack evolution [20–22], 2-D stress analysis using variational method [23] and finite fracture mechanics [24] have been used to simulate matrix cracking in cross-ply laminates. 3-D stress analysis using plane strain assumptions [25] and probabilistic energy based criteria have also been successfully used for matrix crack predictions [26,27]. In addition to these approaches, concept of damage mechanics has been used [28,29]. Crack Opening Displacement (COD) based concepts have also been looked at [30] and crack evolution has been calculated using change in strain energy. Statistical strength based models have also been used to predict crack density evolution [31–36].

Most of the models described here are able to predict matrix crack evolution for simple cross-ply laminates using some form of strength based or energy based criterion and cannot be extended to the more general and more relevant MD-laminates. In MD-laminates, due to the presence of multiple off-axis plies oriented at different angles to the loading direction, the matrix crack evolution is also different in each ply. Few authors have attempted to provide a framework for matrix crack evolution in MD-laminates based on synergistic damage mechanics [19], energy based approach complimented with analytical stress analysis [37,38], 2-D Finite Element Analysis (FEA) with damage constitutive model [39] and more recently, the micro-mechanics based damage model for stiffness reduction with energy based damage evolution [40]. A majority of the approaches described so far employ an energy based criterion for matrix crack initiation and evolution. In-plane uniaxial loading has been considered in most models described here. Recently, crack evolution models under bi-axial loading have been developed [41]. Though statistical strength based theories have been promising in predicting the crack evolution in cross-ply laminates [31–36], no attempt has been made to extend the same to MD-laminates. In this work, a probabilistic strength based framework for matrix crack density evolution and associated stiffness reduction for a symmetric MD-laminate has been presented using oblique coordinate system based stress analysis [36,42,43]. The corresponding stiffness degradation have also been modeled and compared with the available experimental observations in the literature.

2. Matrix crack evolution model

This section describes the methodology adopted to predict matrix crack evolution in a symmetric MD-laminate under in-plane loading. The salient concepts adopted in this study have been listed below.

2.1. Geometry and co-ordinate system

A 2*n* ply symmetric MD-laminate has been considered in this study. A typical k^{th} ply in the MD-laminate has a thickness t_k and length L as depicted in Fig. 1(b). As mentioned in the earlier section, matrix cracks develop along the fiber direction and the crack spacing in any off-axis layer is defined as the distance between two

parallel cracks. Each interior ply has been divided into two halves as shown in Fig. 1(b). The top most and the bottom most plies have been grouped with their respective neighboring half plies while all the interior half plies have been grouped with their corresponding neighboring half plies. In addition, the central plies are grouped together and have not been split into two halves (cf. Fig. 1(b)). Thus, a total of $(2n-2)$ groups of plies have been obtained for the MD-laminate. Utilizing symmetry, the k^{th} and $(2n-1-k)^{th}$ ply groups are assembled as the k^{th} sub-laminate as shown in Fig. 1(b). In general, each sub-laminate will contain arbitrary $[\phi/\varphi]_s$ type lay-up sequence.

2.2. Stress analysis of sub-laminate

The global stresses in each sub-laminate has been estimated using Classical Lamination Plate Theory (CLPT) from the global applied stress, $\bar{\sigma}$. The volume bounded by intersecting planes passing through two neighboring cracks in the adjacent plies of the sub-laminate is chosen to represent the Representative Element (RE) for stress analysis (cf. Fig. 2). The stress distribution in cracked sub-laminate has been estimated using the shear-lag based methodology outlined in Yokozeki et al. [42]. Analytical solutions have been obtained by solving the governing equations using boundary conditions given in (A.13) and (A.14) under applied in-plane loading in oblique coordinate system. To begin with, it is assumed that the laminate under consideration already has initial matrix cracks. Typically, manufacturing induced defects such as voids exist in the composite that result in matrix crack initiation sites [44,45]. Singh et al. [19] have used an Initial Crack Spacing (ICS) of 50 times the thickness of the laminate. In the present analysis, the ICS has been assumed to coincide with the length of the laminate under consideration. For shear-lag analysis, any $[\phi/\varphi]_s$ sub-laminate is mapped onto $[\theta^\circ/90^\circ]_s$ orientation using coordinate transformations. $2l_1$ and $2l_2$ represent the crack spacing (reciprocal of crack density) in θ° and 90°, respectively in the oblique coordinate system for easy handling of limits in (A.13) and (A.14) (cf. Fig. 2). Crack densities in θ° and 90° plies are given by $1/(2l_1\cos\theta)$ and $1/(2l_2\cos\theta)$, respectively. In the oblique coordinate system, covariant components for strain/displacement and contravariant components for stress/force have been used for physically realistic analysis. The in-plane stresses have been assumed to be constant in the thickness direction. The relation between in-plane displacements in each ply (k^{th}) is related to out-of-plane shear stresses at the interface using shear-lag analysis. Appendix A outlines some of the key derivations used in the present analysis [42].

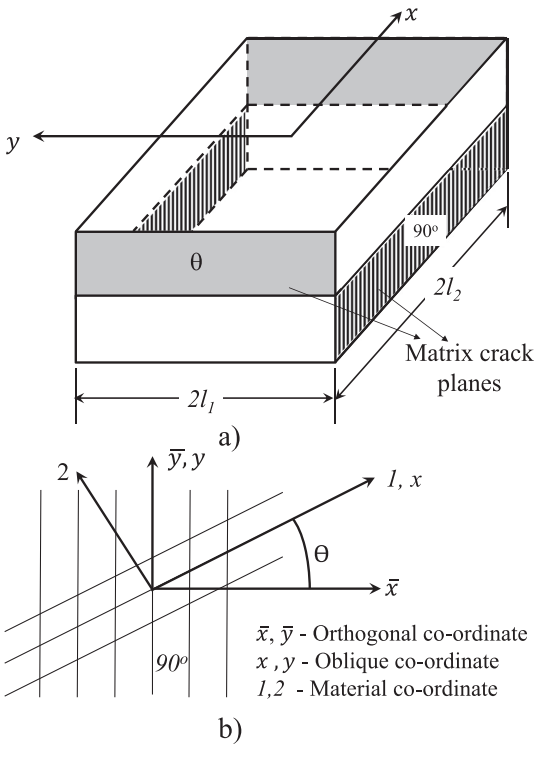

Fig. 2. Representative element for matrix crack evolution model. a) Representative element $[\theta^\circ/90^\circ]_s$, b) Co-ordinate system.

It should be noted that multiple cracks will form in each ply of the sub-laminate during loading. Thus, stress analysis has to be carried out on an array of several RE's as the applied far field loading increases. At higher crack densities, crack interaction effects could occur [43,46]. Additionally, shear lag analysis does not consider the singularity in the stress fields at the crack tip. Since the matrix cracks form instantly throughout the ply thickness and extends throughout the width of the laminate, the stress analysis is limited to the bounded volume without explicitly accounting for the crack tip. Physically, matrix cracks get arrested as they encounter the neighboring ply triggering other damage modes such as delamination. Since the aim of the current work is to develop an analytical framework for matrix cracking in general symmetric MD-laminates, other mechanisms have not been taken into account. The basic assumption involved in shear lag analysis and complexities of MD-laminate cracking are discussed in detail in Ref. [46].

2.3. Material properties and Weibull parameters

$[0/90_8]_s$, $[0/\pm70_4/0_{1/2}]_s$ and $[0/\pm55_4/0_{1/2}]_s$ layups with Fiberite/HyE 9082Af material system (MAT-1) [7], $[0/90]_s$ and $[0/90/\mp45]_s$ layups with Glass roving impregnated with Epikote 828/NMA/BDMA (100:60:1) epoxy-resin system (MAT-2) [8] have been used in the present work. The material properties used in the simulations are shown in Table 1. The Poisson's ratio ν_{23} and shear modulus G_{23} have been estimated using the following expressions [47]:

$$\nu_{23} = \frac{\nu_{12}\left(1 - \frac{E_{22}\nu_{12}}{E_{11}}\right)}{1-\nu_{12}} \tag{1}$$

$$G_{23} = \frac{E_{22}}{2(1+\nu_{23})} \tag{2}$$

It has been observed that there exists a statistical variation in the transverse strength of the ply [48]. In addition, non-uniform crack spacing evolution has been observed during progressive loading that signifies the variation in transverse strength at various material elements (small ply volume on which strength properties are assumed to be uniform) within each off-axis lamina. The strength distribution typically follows a Weibull distribution

Table 1
Material properties for laminates used in the analysis.

Property	Fiberite/HyE9082Af [7]	Glass/Epikote 828 [8]
Ply Thickness, mm	0.14	0.5
$E_{11}(GPa)$	44.7	46.0
$E_{22}(GPa)$	12.7	13.0
$G_{12}(GPa)$	5.8	5.0
ν_{12}	0.30	0.3

[48–50], i.e., the probability of failure of uni-axially loaded material can be expressed as follows:

$$P(Y_t) = 1 - \exp\left[-\left(\frac{Y_t}{\beta}\right)^m\right] \quad (3)$$

where, β is the scale parameter, m is the shape parameter obtained from experiments and Y_t is the transverse strength of the lamina.

It has been observed that transverse strength variation estimated from tensile tests conducted on 90° UD-laminates fail to represent the 'in-situ' transverse strength distribution of the off-axis lamina in constrained MD-laminates [51]. In other words, transverse strength distribution of a particular off-axis ply in a MD-laminate would depend on lamina thickness, material and neighboring constraint ply thicknesses [11]. Such a phenomenon is usually referred to as constraint effect and has been discussed briefly in an earlier section. In order to address this phenomenon, Weibull parameters (in-situ β and m) have been obtained from fitting the experimental data of one 'Master Curve'. The master curve represents the crack density evolution data for a configuration closely resembling that of the laminate (in terms of ply thickness and constraint ply thicknesses) for which predictions need to be made. For example, in the present analysis, $[0/90_8]_s$ [7] is considered as a master curve and used for estimation of Weibull parameters. These Weibull parameters have then been used to predict the crack density evolution in other laminate configurations (e.g., $[0/\pm 70_4/0_{1/2}]_s$) and compared with the experimental values. As can be seen from this example, the constraint effect on the $[\pm 70_4]$ laminae would be similar to that experienced by the $[90_8]$ laminae.

2.4. Compatibility of cracks for evolution

As discussed earlier, cracking in each ply of the sub-laminate occurs in a random fashion depending on the transverse strength assigned to each material element. For a general k^{th} sub-laminate, application of a certain load increment (i^{th} load step) would result in different crack spacings in the neighboring plies (ply-A and ply-B in Fig. 3(a)). In order to estimate the crack spacing evolution for the $(i+1)^{th}$ load step, stress analysis needs to be conducted on a series of RE's. The inconsistent crack spacings in adjacent plies of the sub-laminate makes the selection of the RE's difficult. To this end, the following procedure has been used to determine the crack spacings within a sub-laminate for the next load increment:

1. Average Crack Spacing (ACS) in ply-A and the actual crack spacings in ply-B (B1, B2 … .Bx) from the i^{th} load step yield a set of RE's. Stress analysis is conducted on these RE's to evaluate the crack spacings in ply-B for the $(i+1)^{th}$ load step.
2. ACS of ply-B and the actual crack spacings in ply-A (A1,A2 … Ay) from the i^{th} load step yield another set of RE's. Stress analysis is conducted on these RE's to evaluate the crack spacings in ply-A for the $(i+1)^{th}$ load step.

Thus, the crack spacings in ply-A and ply-B for the $(i+1)^{th}$ load step are determined considering the constraint offered by the neighboring plies within the sub-laminate. In addition, compatibility across sub-laminates also needs to be established at the end of $(i+1)^{th}$ load step. In other words, each ply being shared between two sub-laminates would have non-identical crack spacings. Since each sub-laminate would in general have dissimilar stacking sequences, each half-ply would experience different constraint from its neighboring ply resulting in dissimilar stress distributions; consequently, non-identical crack spacings occur in each half-ply pairs (cf. Fig. 3(b)). Physically, the crack distributions need to be identical in the two-halves of the ply. Thus, at the end of every load increment, the higher average crack density (or, lower average crack spacing) amongst the two halves of the same ply has been assumed to be the crack density of the ply under consideration. Such an approach eliminates the non compatibility arising from sub-laminate type analysis in addition to simulating the conservative constraint effect of the two neighboring plies.

2.5. Stiffness degradation due to matrix cracking

The mathematical description of stiffness estimation for the cracked laminate has been presented in Appendix B based on [52]. The overall effective compliance matrix $\bar{S}$ can been evaluated from the overall effective stiffness matrix outlined in Appendix B. The stiffness properties of the cracked laminate are evaluated using: $E_{\overline{xx}} = 1/\bar{S}_{11}$, $E_{\overline{yy}} = 1/\bar{S}_{22}$, $\nu_{\overline{xy}} = -\bar{S}_{12}/\bar{S}_{11}$, $G_{\overline{xy}} = 1/\bar{S}_{33}$. The uncracked laminate properties are expressed with a subscript 0 (e.g., $E_{\overline{xx}0}$).

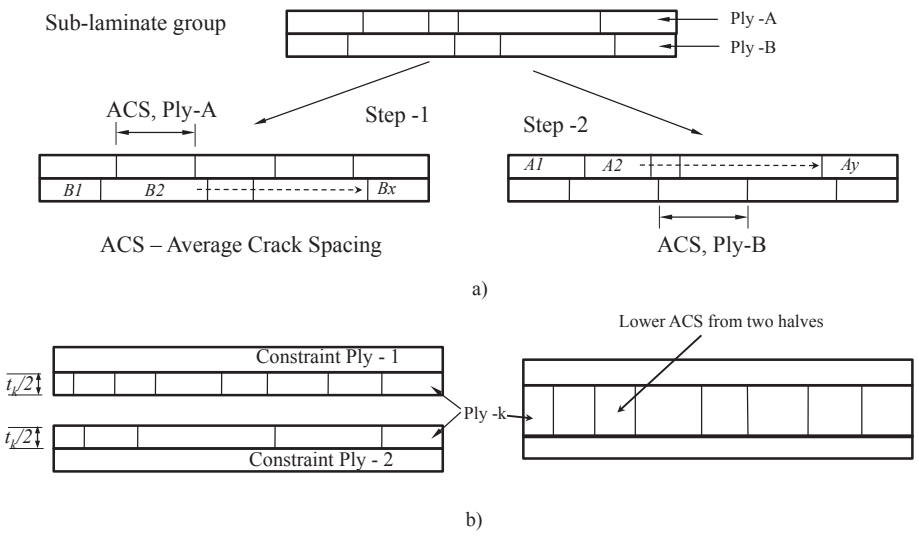

Fig. 3. Representation of matrix crack for stress analysis. a) RE selection for stress analysis b) Compatibility of matrix cracks.

3. Numerical implementation of matrix crack evolution model

Numerical implementation of the matrix cracking evolution in a symmetric MD-laminate has been outlined below:

1. A $2n$ ply symmetric MD-laminate with thickness t and length L subjected to a uniform in-plane external stress field $\bar{\sigma}$ has been chosen for the present analysis (cf. Fig. 1(a)). Orthotropic material properties have been assumed for each lamina. An ICS is chosen to be consistent with the length of the specimen for all the plies in the MD-laminate.
2. Hashin's strength criterion under transverse and shear stresses has been chosen as the failure criterion in the present model. The tensile matrix failure mode is given by:

$$\frac{\sigma_{22}^2}{Y_t^2} + \frac{\tau_{12}^2}{S^2} > = 0 \tag{4}$$

Transverse (Y_t) and shear strengths (S) are assumed to follow Weibull statistical distribution as given in equation (3). Each lamina is divided into N number of material elements and assigned a random strength at the start of the analysis. The cracking of the lamina at a material element is said to occur when equation (4) is met. If not, loading is increased.

3. The MD-laminate has been loaded from zero in increments until saturation crack density has been reached or to the described stress level of interest. At each increment, average global applied stresses in each sub-laminate has been estimated using CLPT.
4. Crack spacing in each lamina has been chosen as per the previous section, to represent the cracked MD-laminate configuration. Stress analysis of the cracked sub-laminate RE is conducted using shear-lag approach. The failure criterion has been checked at every material element using the width averaged stresses and the Weibull strength parameters. The above procedure has been employed for the remaining RE's in the sub-laminates to check for further cracking.
5. Using the above steps, the statistical variation of crack densities in the each ply and the average crack densities have been estimated for the particular load step.
6. Before applying the next load step, the compatibility of crack spacing is checked.

The above methodology is shown Fig. 4.

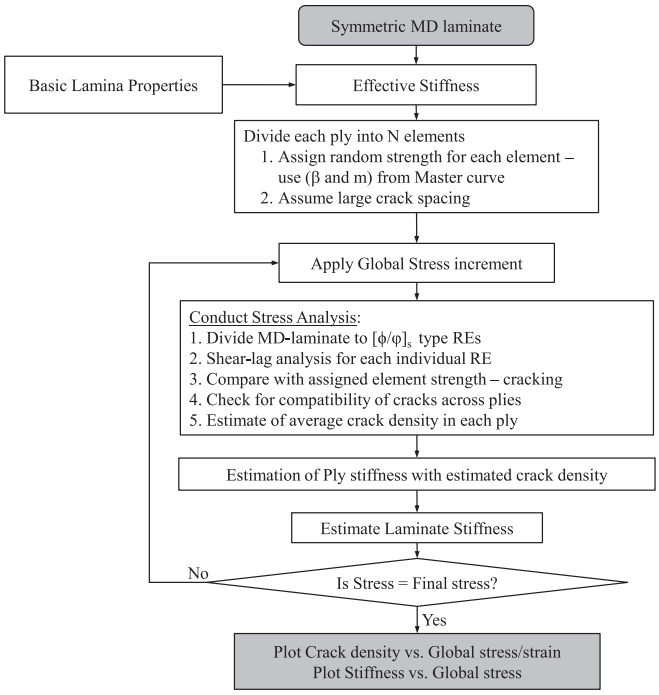

Fig. 4. Flowchart of the proposed methodology for matrix crack evolution in a symmetric MD-laminate.

4. Results and discussion

The analytical framework for probabilistic strength based matrix crack evolution has been implemented in commercial software MATHEMATICA (version 9). Based on the algorithm discussed in the earlier section, predictions for matrix crack evolution and corresponding material property degradation have been carried out.

4.1. Weibull parameters estimation from master curve

Convergence studies were carried out to choose the number of material elements per lamina (N) for transverse strength distribution and the maximum stress increment for matrix crack evolution. It was found that 100,000 material elements and 1 MPa stress increments were sufficient to yield converged solutions. Simulations were also carried out using gage length and half of gage length as ICS to study their sensitivity on crack evolution predictions. The choice of these two ICS did not alter the crack evolution predictions. Thus, the ICS equivalent to length of the specimens have been considered for further study. These converged parameters viz., N = 100,000, 1 MPa stress increments and ICS = length of specimen have been used for all the investigations reported in this work.

It has been observed from the simulations that the shape parameter m controls the rate of crack evolution and the scale parameter β decides the crack initiation strain. At the start of the analysis, an arbitrary β value was chosen and crack density curves were simulated for various values of m. All the crack density curves were overlaid with experimental data and the optimal m value corresponding to the highest correlation coefficient was chosen as the material parameter m. Upon fixing the m value, the optimal β was estimated using trial and error such that the simulated crack initiation point coincided with experimental point. However, it is

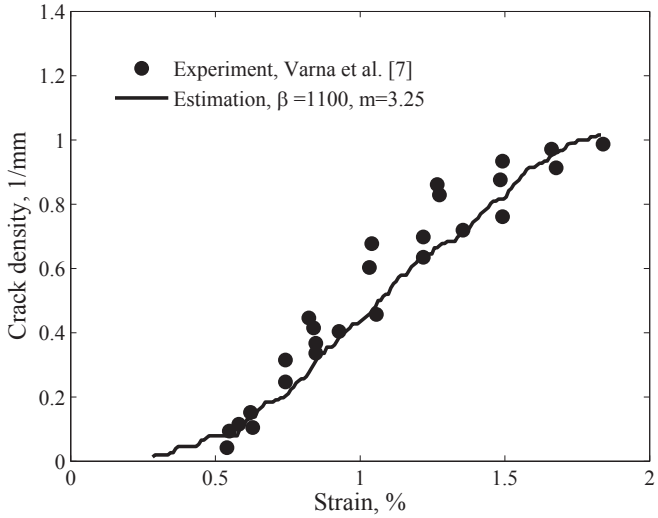

Fig. 5. Determination of fitting parameter for $[0/90_8]_s$ [7] laminate.

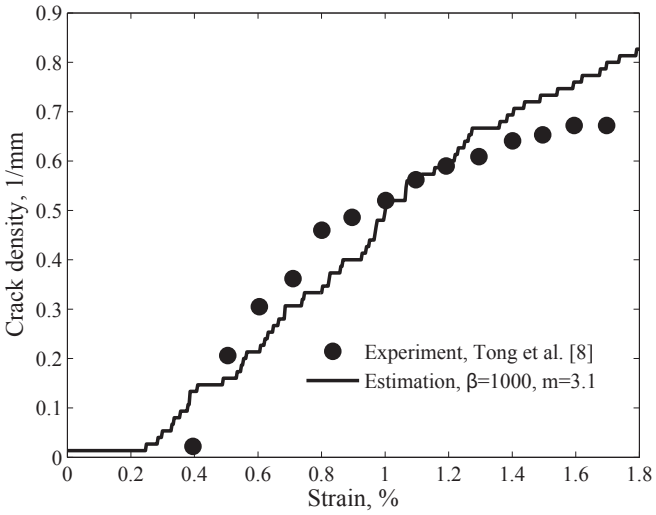

Fig. 6. Determination of fitting parameter for $[0/90]_s$ [8] laminate.

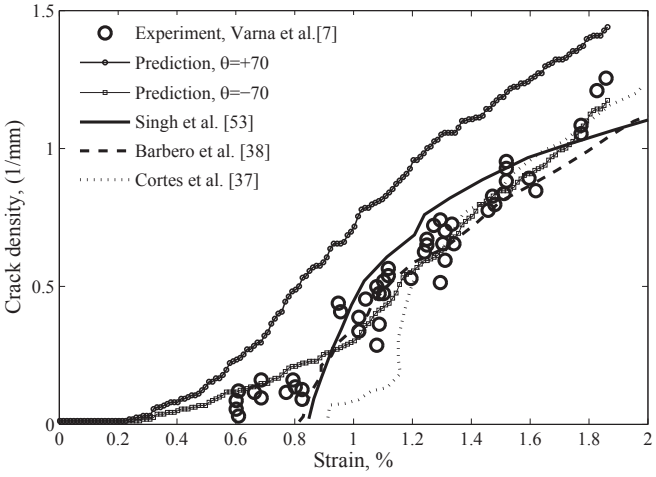

Fig. 7. Comparison of crack density evolution in $[0/\pm70_4/0_{1/2}]_s$ [7] laminate with simulation.

recognized that further studies may be needed to establish an optimum methodology to estimate the Weibull parameters. Fig. 5 and Fig. 6 depict the determination of Weibull parameters for two different materials by fitting the respective master curves for layups $[0/90_8]_s$ [7] and $[0/90]_s$ [8] laminates, respectively. These calibrated values for Weibull parameters have then been used for prediction of crack density evolution for other layups. A note about Weibull shape parameter m: m for autoclave cured carbon fiber composite was experimentally estimated to be 4–6 [49]. In the current study, the MAT-1 considered was produced by autoclave process and MAT-2 was produced by wet layup. MAT-2 may have more variability in the strength as compared to the more controlled autoclave process. The calibrated m values are in the range of reported values. However, the strength indicator β parameter was very high, ≈10 times that of transverse strength observed from experiments. The effect of thickness of the ply and neighboring ply constraint on strength are smeared into a pseudo strength parameter β in this study.

4.2. Crack density evolution

The predicted crack density evolution values for $[+\theta^\circ]$ and $[-\theta^\circ]$ plies of $[0/\pm70_4/0_{1/2}]_s$ and $[0/\pm55_4/0_{1/2}]_s$ are shown in Fig. 7 and Fig. 8. The experimental observations on crack evolution on such laminates were carried out by Varna et al. [7]. The average crack densities have been measured at each $[+\theta^\circ]$ and $[-\theta^\circ]$ with 4 average crack density values reported at each strain level. The variation in these reported (experimental) average crack densities is more than 100% at some strain levels. Thus, it can be inferred that experimental data has a large amount of scatter in addition to different damage levels being present in $[+\theta^\circ]$ and $[-\theta^\circ]$ plies. Predictions by Cortes et al. [37], Barbero et al. [38] and Singh et al. [53] have also been overlaid. As can be seen from the figures, good correlation exists between the predictions and experimental results. It should be noted that similar to the present approach where the in-situ strength of off-axis plies are evaluated via calibration using a master curve, Singh et al. [53] use a 'fit' parameter from a reference configuration. Singh et al.'s approach also requires the estimation of COD and Crack Sliding Displacements (CSD) using FE analysis. These are introduced to evaluate the work needed for the next crack formation. Varna et al. [7] has shown that the average COD at a particular loading has a large scatter. Cortes et al. [37] has assumed equal damage in $[+\theta^\circ]$ and $[-\theta^\circ]$ plies. As can be observed

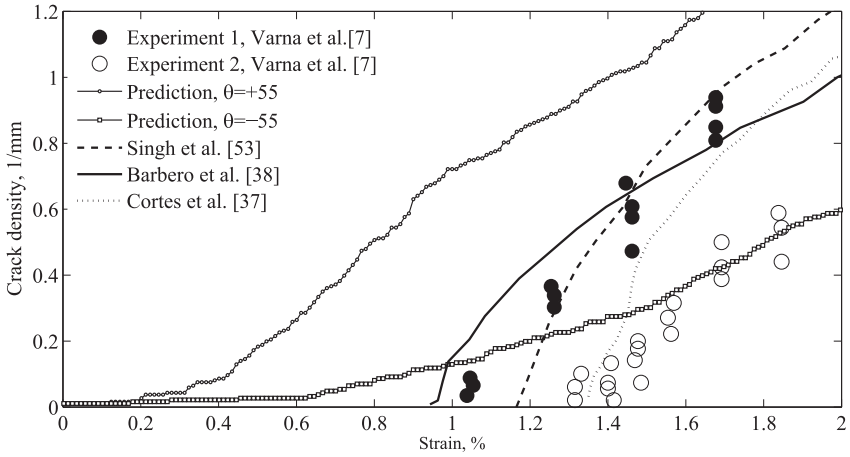

Fig. 8. Comparison of crack density evolution in $[0/\pm55_4/0_{1/2}]_s$ [7] laminate with simulation.

from Fig. 7, crack initiation strains predicted by the current model is less than other models and experimental data. The variations in the ply to ply crack evolution has been captured by the current approach. However, the crack evolution in $[+\theta^\circ]$ ply adjacent to $[0^\circ]$ ply shows higher cracking density than $[-\theta^\circ]$ ply which is constrained by $[0_{1/2}]$. The $[0/+\theta]$ sub-laminate share more load due to higher stiffness than $[-\theta/0_{1/2}]$ sub-laminate from equal strain shared from laminate loading. Overall, it can be concluded that the current approach is yielding a fairly good match with experimental matrix crack density data. Notable observations from the experimental crack density of matrix crack evolution in $[0/\pm55_4/0_{1/2}]_s$ [7] laminate from 2 different tests were reported to fall on 2 different lines with a wide scatter and the authors had mentioned no clear reason for the same.

Experimental observations on matrix crack evolution for $[90^\circ]$ ply in $[0/90/\mp45]_s$ type QI-laminate was carried out by Tong et al. [8]. Crack density predictions for $[0/90/\mp45]_s$ are shown in Fig. 9. The crack density evolution in $[90^\circ]$ ply from simulation using energy approach and 3D-FEM approach [53] have also been overlaid for comparison. Good correlation between experimental and simulation are observed. Again, the crack initiation strains predicted were lesser than experiments. At higher crack densities, the observed QI-laminate behavior was found to deviate from the experimental observations. This may be due to the less constrained contribution from $[\mp45]$ laminate. Singh et al. [53] have pointed out that the actual initial part of the crack evolution curve is curved and shallow rather than starting from a definite initiation point as reported in simulations and experiments. It can be conjectured that the current proposed method is able to capture this phenomenon. Additionally, getting an accurate matrix crack density evolution profile for very small strains would be extremely tedious to conduct experimentally.

The current method assumes a calibrated pseudo transverse strength that smears multiple effects of ply size, constrained effect and the statistical variation. Such an approach can be applied only for laminates with similar to the reference/calibration laminates in terms of constraining plies. The in-plane shear stress induced matrix cracking under static and fatigue loading were reported [7,54]. The in-plane shear strength effect has been ignored in the current simulation. The biggest advantage of the current approach is that being an analytical formulation, predictions can be easily made for all symmetric MD-laminates by simply choosing an

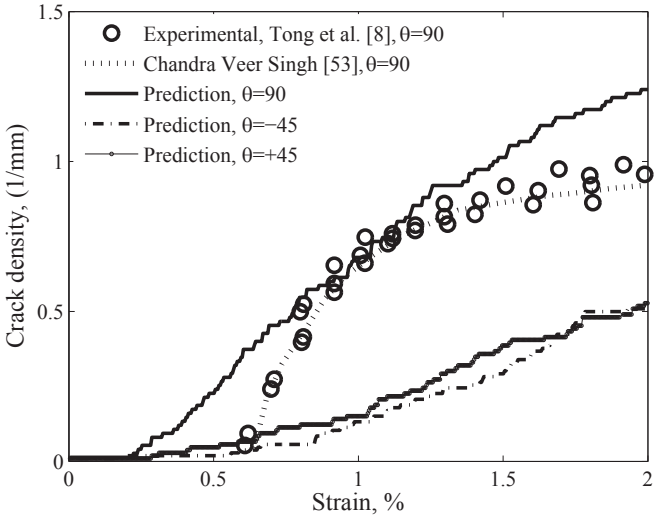

Fig. 9. Comparison for crack density evolution in $[0/90/\mp45]_s$ [8] laminate with simulation.

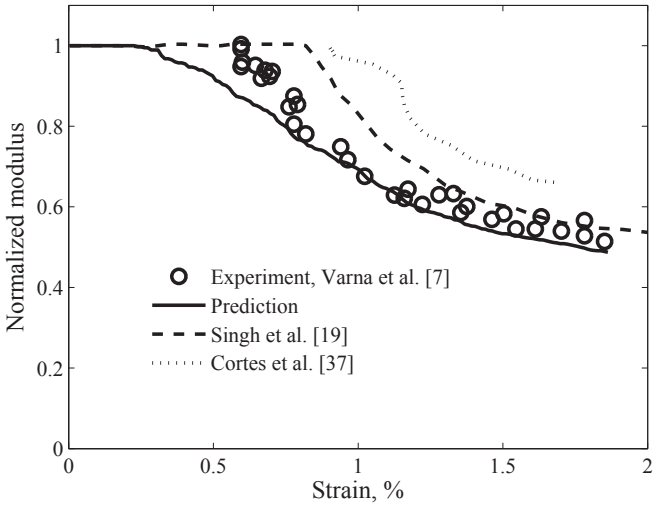

Fig. 10. Normalized axial Young's modulus reduction for $[0/\pm70_4/0_{1/2}]_s$ laminate subjected to uniaxial tensile loading.

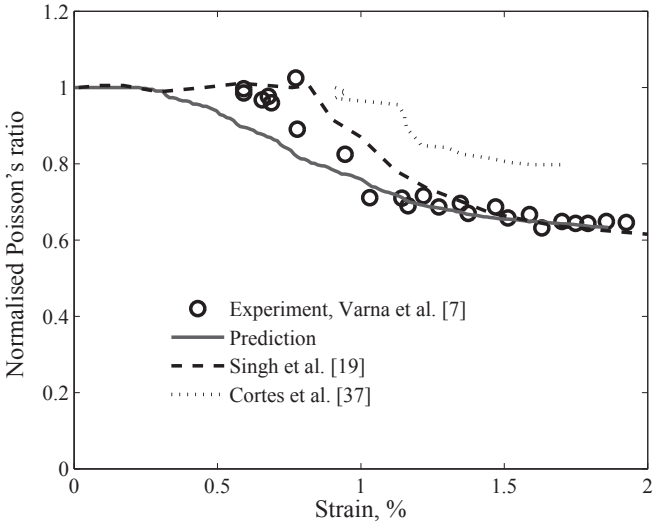

Fig. 11. Normalized Poisson's ratio for $[0/\pm70_4/0_{1/2}]_s$ laminate subjected to uniaxial tensile loading.

appropriate reference configuration. Other approaches such as [53] need careful meshing for various crack configurations to estimate the COD and CSD. In addition, the current approach does not assume equal damage state for $[+\theta^\circ]$ and $[-\theta^\circ]$ plies unlike [37,38,53]. The cross-ply laminate containing different 90 ply thickness has been simulated using Weibull parameters estimated from single [0/90] cross ply laminate and compared with the available literature [11]. However, the matrix crack initiation were not accurately captured by the current model. The in-situ Weibull parameters may be suitable for only the plies of similar thickness in master and the laminate under consideration.

4.3. Mechanical property degradation

As mentioned in the earlier sections, matrix crack density evolution in MD-laminates are accompanied by a degradation in mechanical properties (axial Young's modulus $E_{\overline{xx}}$, axial Poisson's ratio $\nu_{\overline{xy}}$) of the laminate. Varna et al. [7] have reported degraded $E_{\overline{xx}}$ of the laminate for $[0/\pm70_4/0_{1/2}]_s$ and $[0/\pm55_4/0_{1/2}]_s$ configurations

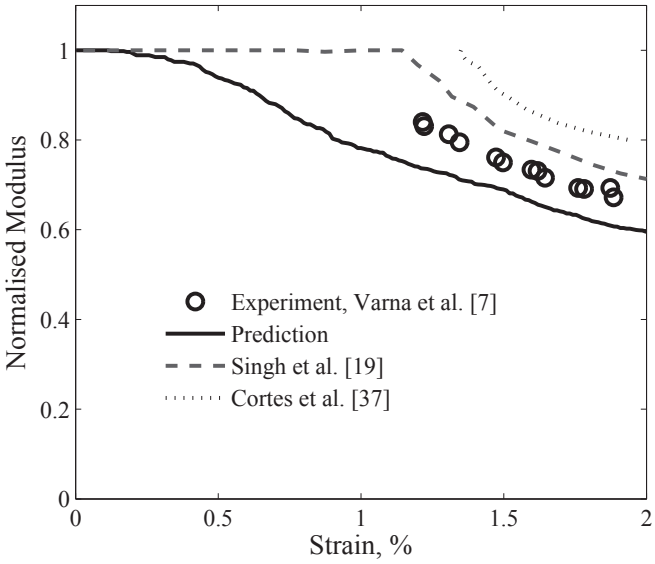

Fig. 12. Normalized axial Young's modulus reduction for $[0/\pm55_4/0_{1/2}]_s$ laminate subjected to uniaxial tensile loading.

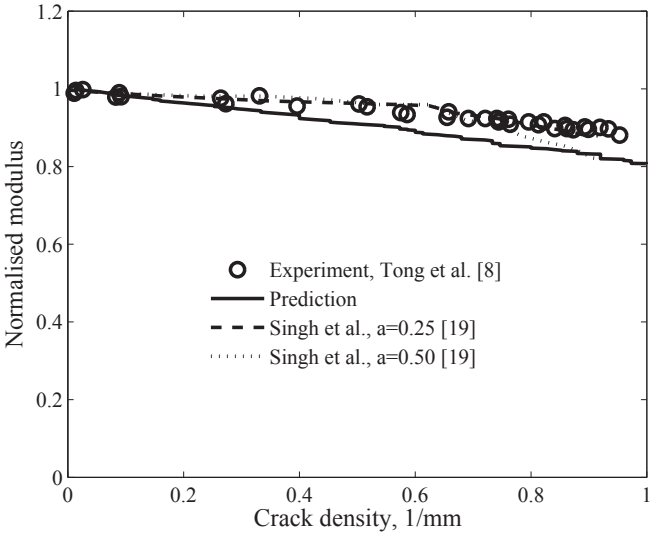

Fig. 14. Normalized axial Young's modulus reduction for $[0/90/\mp45]_s$ laminate subjected to uniaxial tensile loading.

that have been used earlier for crack density evolution. Using the analytical approach discussed in Appendix B, $E_{\overline{xx}}$ and $\nu_{\overline{xy}}$ degradation for $[0/\pm70_4/0_{1/2}]_s$ laminate has been plotted in Figs. 10 and 11. Experimental data by Varna et al. [7] and predictions from Singh et al. [19] and Cortes et al. [37] have also been overlaid with the current model predictions. A close agreement with experiments is observed for normalized $E_{\overline{xx}}$ and $\nu_{\overline{xy}}$ properties of the MD-laminate.

$E_{\overline{xx}}$ and $\nu_{\overline{xy}}$ degradation for $[0/\pm55_4/0_{1/2}]_s$ laminate has been plotted in Figs. 12 and 13. Experimental data [7] and predictions from Singh et al. [19] and Cortes et al. [37] have also been overlaid with the current model predictions. The degradation trend observed in experiments have been accurately captured by the current model. However, an error of approximately 10% for $E_{\overline{xx}}$ value and 5% for $\nu_{\overline{xy}}$ from the experiments were observed. As noted above, large variation in crack densities were seen from 2 different experiments. Wide scatter in such values are expected when large number of experimental data are available for comparison.

Experimental observations on matrix crack evolution and the associated stiffness reduction for $[0/90/\mp45]_s$ type QI-laminate was carried out by Tong et al. [8]. The normalized axial Young's modulus and Poisson's ratio of $[0/90/\mp45]_s$ type laminates predicted using the above methodology under in-plane tensile loading are shown in Fig. 14 and Fig. 15. The normalized property degradation trend for $E_{\overline{xx}}$ and $\nu_{\overline{xy}}$ are closely matching with the experimental results. Maximum error in prediction of 7% in normalized $E_{\overline{xx}}$ value and 6% in $\nu_{\overline{xy}}$ near CDS has been seen. These observations are in line with the crack densities prediction at the higher strain levels, wherein slightly higher crack density values were predicted due to less constraint effect from $[\mp45]$ layer adjacent to $[90^\circ]$ ply in QI-laminate as compared to more constrained master cross-ply laminate. The property degradations predicted using SDM by Singh et al. [19] and the results are superimposed for comparison. In order to account for partial cracks in plies adjacent to $[0^\circ]$, a parameter 'a' (relative density factor) was introduced as a ratio of

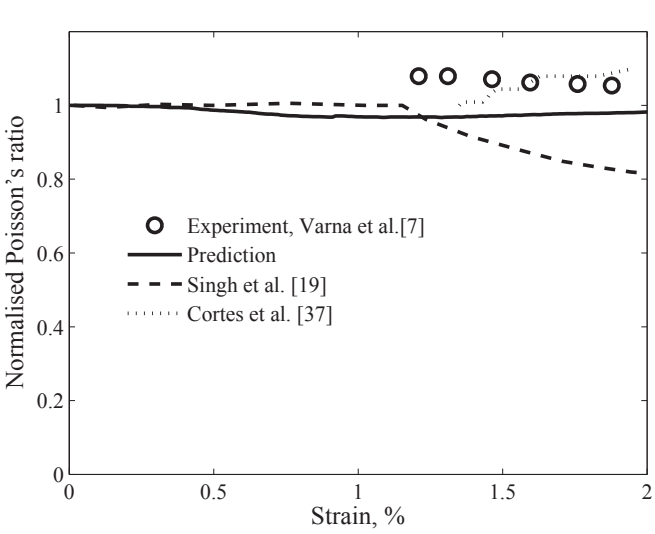

Fig. 13. Normalized Poisson's ratio for $[0/\pm55_4/0_{1/2}]_s$ laminate subjected to uniaxial tensile loading.

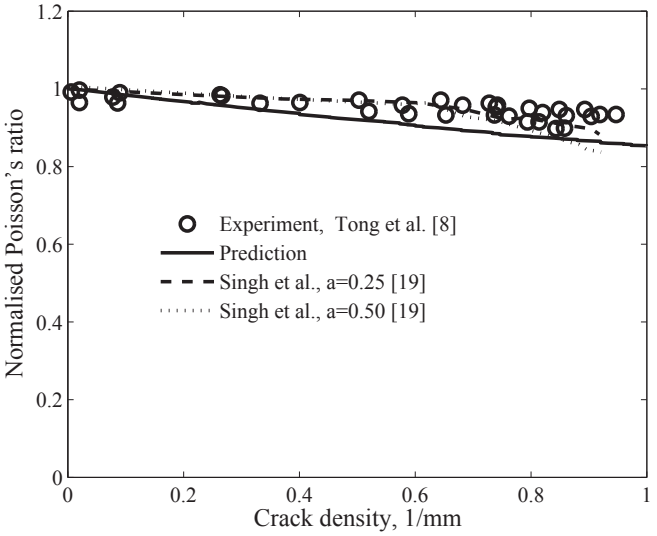

Fig. 15. Normalized Poisson's ratio for $[0/90/\mp45]_s$ laminate subjected to uniaxial tensile loading.

actual surface area of partial cracks to surface area for full cracks by Singh et al. [19].

As seen from the crack evolution curves, the crack evolution in $[+\theta^\circ]$ ply adjacent to $[0^\circ]$ ply shows higher crack density than $[-\theta^\circ]$ ply. The values for crack density do not match the experimental crack density values. The crack density evolution in $[90^\circ]$ ply in QI-laminate show a slightly higher value than experiments due to slight variation in the constraint effect compared to the master laminate. The final stiffness trends predicted closely match the experimental values. However, a maximum error of less than 10% is observed due to slightly higher values of crack densities predicted by the current methodology. It is also noted that all the values predicted by the current model are conservative (higher degradation than experimental), while other models seems to underestimate such trend at some points.

5. Conclusions

An analytical frame work for matrix crack evolution in symmetric MD-laminates subjected to any in-plane static loading has been proposed. A non-deterministic approach to matrix crack evolution has been adopted by considering a statistical distribution of transverse strength. The statistical parameters for Weibull strength distribution has been estimated using a 'master' laminate. The ply-by-ply variations in crack density evolution are predicted. The stiffness properties are also estimated using the above crack density values and compared with the available literature values. The stiffness degradation trend was accurately simulated by the current model and maximum error of less than 10% was observed. The values estimated from the current models are conservative as compared to the other models available in the literature. This method can come in handy for design engineers to perform quick comparisons for different material systems with minimum number of calibration experiments.

Appendix A. Stress analysis of cracked MD-laminate

The coordinate used for the following analysis is shown in Fig. 2(b). Orthogonal coordinate system has been represented by $\bar{x}-\bar{y}-\bar{z}$ and x–y–z represents the oblique coordinate system. The equilibrium equations for (k^{th}) ply (indicated by indices 1 and 2) can be expressed in the through-the-thickness integrated form using stress-strain relation, strain displacement relation and the associated shear lag assumptions. The equilibrium equations in-terms of displacements can be expressed as follows:

The matrix $[T]$ transforms from orthogonal coordinate system to oblique coordinate system:

$$[T]=\begin{bmatrix} \cos^2\theta & \sin^2\theta & 0 & 0 & 0 & \cos\theta\sin\theta \\ 0 & 1 & 0 & 0 & 0 & 0 \\ 0 & 0 & 1 & 0 & 0 & 0 \\ 0 & 0 & 0 & 1 & 0 & 0 \\ 0 & 0 & 0 & \sin\theta & \cos\theta & 0 \\ 0 & 2\sin\theta & 0 & 0 & 0 & \cos\theta \end{bmatrix} \tag{A.1}$$

The stresses and strains in the orthogonal coordinate system can be transformed to oblique coordinate system as follows:

$$\left[\varepsilon_{ij}\right]=[T]\left[\bar{\varepsilon}_{ij}\right] \tag{A.2}$$

$$\left[\sigma^{ij}\right]=[T]^{-T}\left[\bar{\sigma}_{ij}\right] \tag{A.3}$$

The relation between contra-variant stress components and co-variant strain components in the oblique coordinate system can be written as follows:

$$\sigma^{ij}=Q^{ijkl}\left(\varepsilon_{kl}-\varepsilon^0_{kl}\right) \tag{A.4}$$

where, ε_0 represents the initial strain.

The relation between strains and displacements can be written as follows:

$$\varepsilon_{ij}=\frac{1}{2}\left(u_{i,j}+u_{j,i}\right) \tag{A.5}$$

where 4th order contra-variant stiffness components of Q^{ijkl} can be obtained using the following relation:

$$\left[Q^{ijkl}\right]=[T]^{-T}\left[\overline{Q}\right][T]^{-1} \tag{A.6}$$

where $\overline{Q}$ denotes the stiffness matrix in the orthogonal coordinate system.

The in-plane stresses have been assumed to be constant in the thickness direction. The relation between in-plane displacements in each ply (k) is related to out-of-plane shear stresses at the interface using shear-lag analysis as follows [42]:

$$\begin{aligned}\begin{bmatrix}\tau^{(1,2)}_{xz}\\ \tau^{(1,2)}_{yz}\end{bmatrix}&=\begin{bmatrix} sec\theta & 0\\ -tan\theta & 1\end{bmatrix}\left[\overline{C}^{(1,2)}\right]^{-1}\begin{bmatrix} cos\theta & sin\theta\\ 0 & 1\end{bmatrix}^{-1}\begin{bmatrix}u^{(1)}-u^{(2)}\\ v^{(1)}-v^{(2)}\end{bmatrix}\\ &\equiv[H]\begin{bmatrix}u^{(1)}-u^{(2)}\\ v^{(1)}-v^{(2)}\end{bmatrix}\end{aligned} \tag{A.7}$$

where,

$$\left[\overline{C}^{(1,2)}\right]=\frac{t^{(1)}}{3}\begin{pmatrix}\bar{S}^{(1)}_{55} & \bar{S}^{(1)}_{45}\\ \bar{S}^{(1)}_{45} & \bar{S}^{(1)}_{44}\end{pmatrix}+\frac{t^{(2)}}{3}\begin{pmatrix}\bar{S}^{(2)}_{55} & \bar{S}^{(2)}_{45}\\ \bar{S}^{(2)}_{45} & \bar{S}^{(2)}_{44}\end{pmatrix} \tag{A.8}$$

Using the equation (A.7), equilibrium equation can be expressed in terms of in-plane displacements using stress-strain and strain displacement relation:

$$\begin{aligned}\Delta^{(1)}_1u^{(1)}+\Delta^{(1)}_2v^{(1)}&=H_{11}\left(u^{(1)}-u^{(2)}\right)+H_{12}\left(v^{(1)}-v^{(2)}\right),\\ \Delta^{(1)}_2u^{(1)}+\Delta^{(1)}_3v^{(1)}&=H_{21}\left(u^{(1)}-u^{(2)}\right)+H_{22}\left(v^{(1)}-v^{(2)}\right),\\ \Delta^{(2)}_1u^{(2)}+\Delta^{(2)}_2v^{(2)}&=H_{11}\left(u^{(2)}-u^{(1)}\right)+H_{12}\left(v^{(2)}-v^{(1)}\right),\\ \Delta^{(2)}_2u^{(2)}+\Delta^{(2)}_3v^{(2)}&=H_{21}\left(u^{(2)}-u^{(1)}\right)+H_{22}\left(v^{(2)}-v^{(1)}\right)\end{aligned} \tag{A.9}$$

where,

$$\begin{aligned}\Delta^{(k)}_1&=A^{(k)}_{11}\frac{\partial^2}{\partial x^2}+2A^{(k)}_{16}\frac{\partial^2}{\partial x\partial y}+A^{(k)}_{66}\frac{\partial^2}{\partial y^2}\\ \Delta^{(k)}_2&=A^{(k)}_{16}\frac{\partial^2}{\partial x^2}+\left(A^{(k)}_{12}+A^{(k)}_{66}\right)\frac{\partial^2}{\partial x\partial y}+A^{(k)}_{26}\frac{\partial^2}{\partial y^2}\\ \Delta^{(k)}_3&=A^{(k)}_{66}\frac{\partial^2}{\partial x^2}+2A^{(k)}_{26}\frac{\partial^2}{\partial x\partial y}+A^{(k)}_{22}\frac{\partial^2}{\partial y^2}\\ A^{(k)}_{ij}&=t^{(k)}Q^{(k)}_{ij}\end{aligned} \tag{A.10}$$

In order to solve equation (A.9), the following displacement function has been assumed [42]:

$$\begin{pmatrix} u^{(1)} \\ u^{(2)} \\ v^{(1)} \\ v^{(2)} \end{pmatrix} = \begin{pmatrix} a_1 \\ a_2 \\ a_3 \\ a_4 \end{pmatrix} sinh(\lambda x) + \begin{pmatrix} b_1 \\ b_2 \\ b_3 \\ b_4 \end{pmatrix} sinh(\kappa y) + \begin{pmatrix} \varepsilon_x^c \\ \varepsilon_x^c \\ \frac{1}{2}\gamma_{xy}^c \\ \frac{1}{2}\gamma_{xy}^c \end{pmatrix} x + \begin{pmatrix} \frac{1}{2}\gamma_{xy}^c \\ \frac{1}{2}\gamma_{xy}^c \\ \varepsilon_y^c \\ \varepsilon_y^c \end{pmatrix} y \tag{A.11}$$

where, $\varepsilon_x^c, \varepsilon_y^c$ and γ_{xy}^c are unknown constants. Substituting equation (A.11) into (A.9), the solutions may be obtained as an eigenvalue problem. The two positive real set of characteristic values λ_i and κ_i for $i = (1,2)$ and the corresponding eigen vectors can be obtained by using the material properties of the given sub-laminate. Thus, the displacements can be expressed in the following form:

$$\begin{pmatrix} u^{(1)} \\ u^{(2)} \\ v^{(1)} \\ v^{(2)} \end{pmatrix} = \sum_{i=1}^{2} 2C_i \begin{pmatrix} a_{i1} \\ a_{i2} \\ a_{i3} \\ a_{i4} \end{pmatrix} sinh(\lambda x) + \sum_{i=1}^{2} 2D_i \begin{pmatrix} b_{i1} \\ b_{i2} \\ b_{i3} \\ b_{i4} \end{pmatrix} sinh(\kappa y) + \begin{pmatrix} \varepsilon_x^c \\ \varepsilon_x^c \\ \frac{1}{2}\gamma_{xy}^c \\ \frac{1}{2}\gamma_{xy}^c \end{pmatrix} x + \begin{pmatrix} \frac{1}{2}\gamma_{xy}^c \\ \frac{1}{2}\gamma_{xy}^c \\ \varepsilon_y^c \\ \varepsilon_y^c \end{pmatrix} y \tag{A.12}$$

The constants $C_1, C_2, D_1, D_2, \varepsilon_x^c, \varepsilon_y^c$ and γ_{xy}^c are obtained by substituting the displacement equation in strain–displacement equation, stress-strain relation with the appropriate averaged boundary conditions along the crack plane as follows:

$$x = \pm l_2, \begin{cases} \dfrac{1}{2l_1}\displaystyle\int_{-l_1}^{l_1} \sigma^{xx(2)} dy = 0 \\ \dfrac{1}{2l_1}\displaystyle\int_{-l_1}^{l_1} \tau^{xy(2)} dy = 0 \\ \dfrac{1}{2l_1}\displaystyle\int_{-l_1}^{l_1} \sigma^{xx(1)} dy = \dfrac{t^{(1)} + t^{(2)}}{t^{(1)}} \sigma^{xx}, \\ \dfrac{1}{2l_1}\displaystyle\int_{-l_1}^{l_1} \tau^{xy(1)} dy = \dfrac{t^{(1)} + t^{(2)}}{t^{(1)}} \tau^{xy} \end{cases} \tag{A.13}$$

$$y = \pm l_1, \begin{cases} \dfrac{1}{2l_2}\displaystyle\int_{-l_2}^{l_2} \sigma^{yy(1)} dx = 0, \\ \dfrac{1}{2l_2}\displaystyle\int_{-l_2}^{l_2} \tau^{xy(1)} dx = 0 \\ \dfrac{1}{2l_2}\displaystyle\int_{-l_2}^{l_2} \sigma^{yy(2)} dx = \dfrac{t^{(1)} + t^{(2)}}{t^{(2)}} \sigma^{yy}, \\ \dfrac{1}{2l_2}\displaystyle\int_{-l_2}^{l_2} \tau^{xy(2)} dx = \dfrac{t^{(1)} + t^{(2)}}{t^{(2)}} \tau^{xy} \end{cases} \tag{A.14}$$

where, $\sigma^{xx}, \sigma^{yy}, \tau^{xy}$ are the applied far-field stress on the sub-laminate in oblique coordinate system. Once the constants are known, using equation (A.4), (A.5) and (A.12), the stresses in the laminate can be obtained.

Appendix B. Stiffness predictions of cracked MD-laminate

Once the displacements in the cracked $[\theta_m/90_n]_s$ sub-laminate equation (A.12) is estimated, the effective strains in the un-cracked boundary can be expressed as:

$$\widetilde{\varepsilon}_{ij} = \frac{1}{V}\int_s u_i n_j ds \tag{B.1}$$

The effective in-plane strains can be expressed as [43]:

$$\begin{aligned} \widetilde{\varepsilon}_{xx} &= \frac{1}{4l_1 l_2}\int_{-l_1}^{l_1} \left(u^{(1)}|_{x=l_2} - u^{(1)}|_{x=-l_2}\right) dy, \\ \widetilde{\varepsilon}_{yy} &= \frac{1}{4l_1 l_2}\int_{-l_2}^{l_2} \left(v^{(2)}\Big|_{y=l_1} - v^{(2)}\Big|_{y=-l_1}\right) dx, \\ \widetilde{\gamma}_{xy} &= \frac{1}{4l_1 l_2}\left[\int_{-l_1}^{l_1} \left(v^{(1)}|_{x=l_2} - v^{(1)}|_{x=-l_2}\right) dy + \int_{-l_2}^{l_2} \left(u^{(2)}\Big|_{y=l_1} - u^{(2)}\Big|_{y=-l_1}\right) dx\right] \end{aligned} \tag{B.2}$$

The overall stiffness properties of a given $[\theta_m/90_n]_s$ sublaminate can be obtained by applying unit in-plane stresses individually as three cases:

$$\begin{aligned} &a)[\sigma^{xx} \quad \sigma^{yy} \quad \tau^{xy}]^T = [1 \quad 0 \quad 0]^T \\ &b)[\sigma^{xx} \quad \sigma^{yy} \quad \tau^{xy}]^T = [0 \quad 1 \quad 0]^T \\ &c)[\sigma^{xx} \quad \sigma^{yy} \quad \tau^{xy}]^T = [0 \quad 0 \quad 1]^T \end{aligned} \tag{B.3}$$

The three effective in-plane strains are obtained as $\widetilde{\varepsilon}_{xx}^m, \widetilde{\varepsilon}_{yy}^m, \widetilde{\gamma}_{xy}^m, (m = a, b, c)$. The effective compliance matrix in the oblique coordinate system can be expressed as follows:

$$\left[\widetilde{S}_{ijkl}\right] = \begin{bmatrix} \widetilde{\varepsilon}_x^{(a)} & \widetilde{\varepsilon}_x^{(b)} & \widetilde{\varepsilon}_x^{(c)} \\ \widetilde{\varepsilon}_y^{(a)} & \widetilde{\varepsilon}_y^{(b)} & \widetilde{\varepsilon}_y^{(c)} \\ \widetilde{\nu}_{xy}^{(a)} & \widetilde{\nu}_{xy}^{(b)} & \widetilde{\nu}_{xy}^{(c)} \end{bmatrix} \tag{B.4}$$

The effective compliance matrix in orthogonal coordinate system can be estimated from coordinate transformation and the effective stiffness matrix can also be estimated from the reciprocal of compliance matrix. Then, the overall stiffness properties of the MD-laminate can be obtained using the sub-laminate properties and classical lamination theory as follows:

$$\left[\overline{Q}\right] = \frac{\sum_{k=1}^{n-1} t^{(k)} \overline{Q}^{(k)}}{\sum_{k=1}^{n-1} t^{(k)}} \tag{B.5}$$

References

[1] Roeseler WG, Sarh B, Kismarton M, Quinlivan J, Sutter J, Roberts D. Composite structures: the first 100 years. In: 16th international conference on composite materials; 2007.
[2] Renton WJ, Olcott D, Roeseler W, Batzer R, Baron W, Velicki A. Future of flight vehicle structures (2000 to 2023). J Aircr 2004;41:986–98.
[3] Degrieck J, Van Paepegem W. Fatigue damage modeling of fibre-reinforced composite materials: review. Appl Mech Rev 2001;54(4):279–330.
[4] Harris B. Fatigue in composites: science and technology of the fatigue response of fibre-reinforced plastics. Woodhead Publishing; 2003.
[5] Abrate S. Matrix cracking in laminated composites: a review. Compos Eng 1991;1(6):337–53.
[6] Reifsnider K, Talug A. Analysis of fatigue damage in composite laminates. Int J Fatigue 1980;2(1):3–11.
[7] Varna J, Joffe R, Akshantala N, Talreja R. Damage in composite laminates with off-axis plies. Compos Sci Technol 1999;59(14):2139–47.
[8] Tong J, Guild F, Ogin S, Smith P. On matrix crack growth in quasi-isotropic laminates – 1. Experimental investigation. Compos Sci Technol 1997;57(11):1527–35.
[9] Yokozeki T, Aoki T, Ogasawara T, Ishikawa T. Effects of layup angle and ply thickness on matrix crack interaction in contiguous plies of composite laminates. Compos Part A Appl Sci Manuf 2005;36(9):1229–35.
[10] Yokozeki T, Aoki T, Ishikawa T. Consecutive matrix cracking in contiguous plies of composite laminates. Int J Solids Struct 2005;42(9):2785–802.
[11] Nairn JA. Matrix microcracking in composites. Compr Compos Mater 2000;2(12):403–32.
[12] Garrett K, Bailey J. Multiple transverse fracture in 90 cross-ply laminates of a glass fibre-reinforced polyester. J Mater Sci 1977;12(1):157–68.
[13] Parvizi A, Bailey J. On multiple transverse cracking in glass fibre epoxy cross-ply laminates. J Mater Sci 1978;13(10):2131–6.
[14] Parvizi A, Garrett K, Bailey J. Constrained cracking in glass fibre-reinforced epoxy cross-ply laminates. J Mater Sci 1978;13(1):195–201.
[15] Bailey J, Curtis P, Parvizi A. On the transverse cracking and longitudinal splitting behaviour of glass and carbon fibre reinforced epoxy cross ply laminates and the effect of poisson and thermally generated strain. Proc Royal Soc Lond A Math Phys Sci 1979;366(1727):599–623.
[16] Flaggs DL, Kural MH. Experimental determination of the in situ transverse lamina strength in graphite/epoxy laminates. J Compos Mater 1982;16(2):103–16.
[17] Groves S, Harris C, Highsmith A, Allen D, Norvell R. An experimental and analytical treatment of matrix cracking in cross-ply laminates. Exp Mech 1987;27(1):73–9.
[18] Hu S, Bark JS, Nairn JA. On the phenomenon of curved microcracks in [(s)/90n] s laminates: their shapes, initiation angles and locations. Compos Sci Technol 1993;47(4):321–9.
[19] Singh CV. Multiscale modeling of damage in multidirectional composite laminates. Ph.D. thesis. Texas A&M University; 2008.
[20] Nairn JA. On the use of shear-lag methods for analysis of stress transfer in unidirectional composites. Mech Mater 1997;26(2):63–80.
[21] Rosen BW. Tensile failure of fibrous composites. AIAA J 1964;2(11):1985–91.
[22] Laws N, Dvorak GJ. Progressive transverse cracking in composite laminates. J Compos Mater 1988;22(10):900–16.
[23] Hashin Z. Analysis of cracked laminates: a variational approach. Mech Mater 1985;4(2):121–36.
[24] Hashin Z. Finite thermoelastic fracture criterion with application to laminate cracking analysis. J Mech Phys Solids 1996;44(7):1129–45.
[25] McCartney L. Analytical models of stress transfer in unidirectional composites and cross-ply laminates, and their application to the prediction of matrix/transverse cracking. In: Local mechanics concepts for composite material systems. Springer; 1992. p. 251–82.
[26] McCartney L. Predicting transverse crack formation in cross-ply laminates. Compos Sci Technol 1998;58(7):1069–81.
[27] Vinogradov V, Hashin Z. Probabilistic energy based model for prediction of transverse cracking in cross-ply laminates. Int J Solids Struct 2005;42(2):365–92.
[28] Talreja R. A continuum mechanics characterization of damage in composite materials. Proc Royal Soc Lond A Math Phys Sci 1985;399(1817):195–216.
[29] Ladeveze P. A damage computational method for composite structures. Comput Struct 1992;44(1):79–87.
[30] Gudmundson P, Weilin Z. An analytic model for thermoelastic properties of composite laminates containing transverse matrix cracks. Int J Solids Struct 1993;30(23):3211–31.
[31] Hahn H, Tsai S. On the behavior of composite laminates after initial failures. J Compos Mater 1974;8(3):288–305.
[32] Fukunaga H, Chou T-W, Peters P, Schulte K. Probabilistic failure strength analyses of graphite/epoxy cross-ply laminates. J Compos Mater 1984;18(4):339–56.
[33] Fukunaga H, Chou T-W, Schulte K, Peters P. Probabilistic initial failure strength of hybrid and non-hybrid laminates. J Mater Sci 1984;19(11):3546–53.
[34] Peters P. The strength distribution of 90 plies in 0/90/0 graphite-epoxy laminates. J Compos Mater 1984;18(6):545–56.
[35] Manders PW, Chou T-W, Jones FR, Rock JW. Statistical analysis of multiple fracture in 0/90/0 glass fibre/epoxy resin laminates. J Mater Sci 1983;18(10):2876–89.
[36] Sun Z, Luo J-J, Daniel I. A novel statistical model for predicting matrix cracking in high temperature polymer composite laminates. J Mater Sci 2003;38(14):3029–35.
[37] Cortes DH, Barbero EJ. Stiffness reduction and fracture evolution of oblique matrix cracks in composite laminates. Ann Solid Struct Mech 2010;1(1):29–40.
[38] Barbero EJ, Cortes DH. A mechanistic model for transverse damage initiation, evolution, and stiffness reduction in laminated composites. Compos Part B Eng 2010;41(2):124–32.
[39] Barbero E, Sgambitterra G, Adumitroaie A, Martinez X. A discrete constitutive model for transverse and shear damage of symmetric laminates with arbitrary stacking sequence. Compos Struct 2011;93(2):1021–30.
[40] Sadeghi G, Hosseini-Toudeshky H, Mohammadi B. An investigation of matrix cracking damage evolution in composite laminates–development of an advanced numerical tool. Compos Struct 2014;108:937–50.
[41] Montesano J, Singh CV. Predicting evolution of ply cracks in composite laminates subjected to biaxial loading. Compos Part B Eng 2015;75:264–73.
[42] Yokozeki T, Aoki T. Stress analysis of symmetric laminates with obliquely-crossed matrix cracks. Adv Compos Mater 2004;13(2):121–40.
[43] Yokozeki T. Simplified method for predicting overall thermomechanical properties of cracked composite laminates. J Reinf Plastics Compos 2010;29(5):675–84.
[44] Lambert J, Chambers A, Sinclair I, Spearing S. 3D damage characterisation and the role of voids in the fatigue of wind turbine blade materials. Compos Sci Technol 2012;72(2):337–43.
[45] Huang Y. Damage evolution in laminates with manufacturing defects. Ph.D. thesis. Sweden: Luleå University of Technology; 2013.
[46] Talreja R, Singh CV. Damage and failure of composite materials. Cambridge University Press; 2012.
[47] Hashin Z. Analysis of composite materials: a survey. J Appl Mech 1983;50(3):481–505.
[48] Sun Z, Daniel I, Luo J. Statistical damage analysis of transverse cracking in high temperature composite laminates. Mater Sci Eng A 2003;341(1):49–56.
[49] Huang Y, Varna J, Talreja R. Statistical methodology for assessing manufacturing quality related to transverse cracking in cross ply laminates. Compos Sci Technol 2014;95:100–6.
[50] Huang Y, Talreja R. Statistical analysis of oblique crack evolution in composite laminates. Compos Part B Eng 2014;65:34–9.
[51] Camanho PP, Dávila CG, Pinho ST, Iannucci L, Robinson P. Prediction of in situ strengths and matrix cracking in composites under transverse tension and in-plane shear. Compos Part A Appl Sci Manuf 2006;37(2):165–76.
[52] Yokozeki T, Aoki T. Overall thermoelastic properties of symmetric laminates containing obliquely crossed matrix cracks. Compos Sci Technol 2005;65(11):1647–54.
[53] Singh CV, Talreja R. Evolution of ply cracks in multidirectional composite laminates. Int J Solids Struct 2010;47(10):1338–49.
[54] Quaresimin M, Susmel L, Talreja R. Fatigue behaviour and life assessment of composite laminates under multiaxial loadings. Int J Fatigue 2010;32(1):2–16.